

A Particle Interaction Model for the Simulation of Biological, Cross-Linked Fiber Networks Inspired From flocking Theory

RICARDO ALONSO,^{1,2} JENNIFER YOUNG,¹ and YINGDA CHENG³

¹Department of Computational and Applied Mathematics, Rice University, 6100 Main MS-134, Houston, TX 77005, USA; ²Departamento de Matemática, PUC-Rio, Rio de Janeiro, Brazil; and ³Department of Mathematics, Michigan State University, 619 Red Cedar Road, East Lansing, MI 48824, USA

(Received 28 May 2013; accepted 26 September 2013)

Associate Editor Michael R. King oversaw the review of this article.

Abstract—Dynamic, cross-linked, biological fiber networks play major roles in cell and tissue function. They are challenging structures to model due to the vast number of components and the complexity of the interactions within the structure. We present here a particle-based model for fiber networks inspired from flocking theory, where fibers are modeled as point particles and cross-link interactions are modeled *via* distance-based potential functions. The frictional potential in flocking models takes on the form of a function that decays with increasing inter-particle distance, with the specific form of this function fit for a particular model. We determined, by conducting full microscopic fiber network simulations, that for the case of a cross-linked fiber network, this function takes on the form of a Gaussian. The basic flocking model is also modified to include an elastic potential as well as drag from the surrounding fluid. Conceptually, the proposed model can be understood as a distributed *Kelvin–Voigt* particle model. The model is able to simulate behaviors such as strain hardening, viscoelastic creep, stress relaxation, network rupture, and network reformation, which are common characteristics of biological fiber networks. The numerical experiments shown in this paper utilize experimentally-derived parameters for actin fiber networks (as a test case), and produce biologically reasonable results. The benefits of this particle model over polymer-based models are that they are computationally simple to implement and can be easily connected to kinetic and continuum-level models.

Keywords—Biological networks, Actin fiber network, Mesoscopic scale, Kelvin–Voigt model, Biomechanics, Viscoelasticity, Cytoskeleton.

INTRODUCTION

Biological fiber networks such as the actin filament network of the cytoskeleton and the collagen-elastin

network of the extracellular matrix are complex cross-linked structures that provide internal and external mechanical support to cells.^{1,6} These networks are often dynamic, capable of breaking and reforming protein cross-links to rearrange their structures,^{1,4,46} giving cells and tissue the ability to substantially change shape and adapt in response to external and internal, mechanical and biochemical stimuli.^{1,20,37}

Because of the significance of fibrous networks in cell and tissue functions, there is a great deal of interest in modeling these complex structures. However, creating discrete models is computationally challenging due to the large number of individual components in the network. Many research groups have taken one of three main approaches to model structures of this nature. The first is to create a detailed discrete model of all fibers (modeled as beams, semi-flexible polymers, or even at the level of monomers²⁸), and cross-links (modeled as springs), but one that represents a small portion of the whole network, and thus contains a computationally manageable number of components.^{4,7,12,20,23,28} The second approach is to treat the network as a continuous medium, modeled in various ways such as a viscoelastic material,²⁷ a porous or poroelastic medium,^{14,42} a two-phase viscous fluid,² or an active gel.^{26,9} The third approach is a compromise between the first two, where coarse-graining and/or homogenization methods are utilized to create a less detailed, regularly-patterned discrete model, that represents the whole network.^{32,40,29} The first approach provides a detailed but spatially limited model of the fiber structure. The second and third methods can be utilized to model the network for a larger domain, but the challenge lies in constructing accurate constitutive laws or homogenization techniques that encompass the dynamic and heterogeneous nature of the fiber network.

Address correspondence to Ricardo Alonso, Department of Computational and Applied Mathematics, Rice University, 6100 Main MS-134, Houston, TX 77005, USA. Electronic mail: rja2@rice.edu

In this work, we take a different approach and present a particle-interaction model for biological, fibrous networks that is inspired from flocking theory.^{19,11} The term *flocking* refers to individuals moving together in an ordered motion via interactions with each other and their environment.¹⁹ Cross-linked fiber networks can be viewed as a *flock*, with the fibers as the individuals and the cross-links as means of interaction. In this mesoscopic model, fibers are represented as point particles, and the cross-link interactions are modeled with potentials. The frictional potential in a basic flocking model¹⁹ is a function that decays with increasing inter-particle distance. It was determined that in the context of a cross-linked fiber network, a Gaussian is an appropriate choice for this function's shape. An elastic potential and drag term are also added to the basic flocking model to capture close neighbor interactions and interstitial fluid friction.

There are several computational and theoretical advantages to such a model. First of all, through the use of distance-based potentials, one can avoid the task of keeping track of which fiber is connected to which other fiber (which is the case for the polymer models of Aström *et al.*,⁴ Head *et al.*,²⁰ and Huisman *et al.*²³). Secondly, in comparison with polymer models where fibers are represented as multi-segmented chains,^{4,20,23} the representation of fibers as particles reduces greatly the number of variables needed to describe each fiber and thus the system (similar to rigid rods models previously suggested^{44,30}). As we will demonstrate, this reduction does not prevent the model from capturing experimentally observed, fiber network behaviors. Another advantage is that there is no need for boundary tracking, thus, a particle model is simple to couple with other physical phenomena, for example an exterior membrane or an interior fluid domain. These advantages make the code development effort relatively low and the code itself computationally inexpensive. Theoretically, this model has rigorous conservation of mass and momentum. Thermal variations can be easily introduced using Brownian motion (a thermostat). Also it should be noted that this model is fully deterministic. Initial conditions are described for all fibers and external forces, then the system is evolved forward in time with no further intervention.

We note here that our approach resembles the method of dissipative particle dynamics (DPD) developed to simulate meso-scale phenomena, for instance, polymers solutions, gels and membranes.^{22,18} In DPD the particles represent clusters of atoms or molecules, likewise, our particles represent actin filaments of a fixed typical length. Computationally speaking, DPD takes advantage of the *soft* particle-particle interactions. This is precisely the case for the biological networks as well where the interactions between fibers are strong at short

range but decay rapidly at longer distances. However, our approach differs from DPD in the fact that we introduce a hybrid model, that is, we use first principles for the conservative forces and a phenomenological model¹¹ for the dissipative forces. Below, we will show that the model presented can be understood as a distributed *Kelvin–Voigt* particle model.

Evidently the simplifications used in the model, such as the fiber rigidity assumption, introduce scale related limitations to it. The model overlooks fine phenomena occurring at the *fiber scale* such as hydrodynamic interactions between fibers due to fiber deformation and motion, nonuniform viscous drag in individual fibers due to hydrodynamic screening which leads to additional fiber bending,¹³ and other bending related phenomena. We stress, however, that the strength of the proposed model relies in the fact that it is able to capture cumulative effects of such fine scale at the *cell scale* with relatively low computational cost. In this way, hydrodynamic interactions can accurately be considered at the cell scale by coupling the model for example with Stoke's equation.

In the next section, we present a detailed description of the particle-potential model equations. To demonstrate the model's capabilities we will choose an actin filament network as a test case. The structure and parameter values for an actin fiber network will be described. We then test our model's ability to capture behaviors such as strain hardening, viscoelastic creep, stress relaxation, network rupture and network reformation. The model will also be used to investigate whether mechanical energy can propagate in an actin fiber network when external forces are applied. Finally, an overall discussion of the model, results and future work will be presented.

MATHEMATICAL MODEL

Our model consists of a cross-linked system of n fibers evolving in the plane \mathbb{R}^2 . Each fiber is assigned a length L and mass m , (lumped into two masses ($m/2$) at its two end points). Each fiber i , $1 \leq i \leq n$, is described by its center of mass position vector $\mathbf{x}_i = \langle x_1, x_2 \rangle \in \mathbb{R}^2$ and center of mass velocity vector $\mathbf{v} = \langle v_1, v_2 \rangle \in \mathbb{R}^2$. Fibers also have an orientation angle denoted by $\theta_i \in [-\pi/2, \pi/2]$ with associated angular velocity $\omega_i \in \mathbb{R}$. In the case of fibers moving in the plane, θ_i is simply the angle between the filament and the horizontal axis (see Fig. 1 (left)).

In principle, free moving fibers follow simple physical laws of fluid dynamics, however, what make them special is their interaction with close neighbors *via* cross-links. We propose here a modified Cucker–Smale model¹¹ for the description of the evolution of the fiber

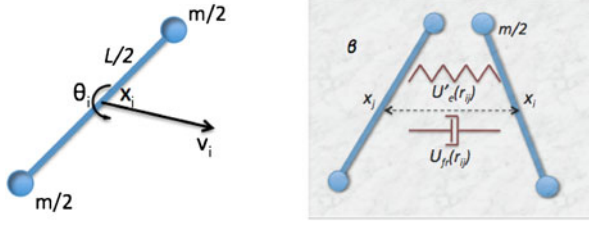


FIGURE 1. Model of a fiber as a rigid rod (left). The interaction model (right) is conceptually a Kelvin–Voigt model between any interacting fiber pair having viscosity $\frac{\lambda_1}{n} U'_{fr}(r_{ij})$, elasticity $\frac{\lambda_2}{n} U'_e(r_{ij})$ and underlying drag β .

network. The equations for the evolution of the center of mass position \mathbf{x}_i and velocity \mathbf{v}_i for the i^{th} -fiber, $1 \leq i \leq n$ are:

$$\frac{d\mathbf{x}_i}{dt} = \mathbf{v}_i \quad (1a)$$

$$m \frac{d\mathbf{v}_i}{dt} = -\beta_1 \mathbf{v}_i - \frac{\lambda_1}{n} \sum_{j=1}^n U'_{fr}(r_{ij})(\mathbf{v}_i - \mathbf{v}_j) - \frac{\lambda_2}{n} \sum_{j=1}^n U'_e(r_{ij}) \frac{\mathbf{x}_i - \mathbf{x}_j}{r_{ij}} + \mathbf{F}(t, \mathbf{x}_i). \quad (1b)$$

The term $\beta_1 \mathbf{v}_i$ represents drag forces from an interstitial fluid (for example, cytosol within the cell) on the fiber where β_1 is the drag coefficient, computed using slender body theory. The quantities $U'_{fr}(r_{ij})$ and $U'_e(r_{ij})$ are the friction and elastic potentials, that are computed based on $r_{ij} = |\mathbf{x}_i - \mathbf{x}_j|$, the distance between fibers i and j . The sum with $U'_{fr}(r_{ij})$ should be thought of as representing the total frictional force from the interaction between neighboring fibers that produces a tracking phenomenon. That is, the velocity \mathbf{v}_i tracks a weighted average of its cross-linked fibers' velocities. The parameter λ_1 is related to the friction coefficient for the fibers. Intuition tells us that the potential $U'_{fr}(r_{ij})$ should be a function that decays as r_{ij} increases, likely vanishing after several fiber lengths L . We propose that $U'_{fr}(r_{ij})$ takes the form of a Gaussian:

$$U'_{fr}(r_{ij}) = \frac{1}{\sqrt{2\pi}\sigma^2} e^{-\frac{r_{ij}^2}{2\sigma^2}}$$

where σ is the standard deviation. To validate this choice, we ran a fully microscopic simulation of a fiber network. By fully microscopic we mean: (1) each fiber is modeled as a chain of masses and springs, (2) cross-links between fibers are also modeled as springs and can form between any two segments of fibers i and j if these segments are within a given distance R of one another. We create the initial fiber network by randomly placing and orienting M fibers each with S segments in a square domain (for this demo, $M = 500$,

$S = 10$). Cross-links between fibers are established by checking the distance between each of the 10 segments of fiber i and all segments on fiber j where $i \neq j$. In its initial state the fiber network is assumed to be in mechanical equilibrium and have a potential energy of zero (all springs are at their relaxed lengths).

To isolate the effect that one fiber's movement has on the rest of the network, we move one centrally located fiber (with a random motion) and observe the network's reaction to this break from equilibrium. The motion of the fiber network is determined by setting up and simulating a large ODE system containing $4 \cdot M \cdot (S + 1)$ equations (x and y position equations, and x and y velocity equations for all fiber segment endpoints).

To establish the influence of the relocation of this central fiber with respect to the rest of the fibers in the system, we create a scatter plot of each fiber's distance from the central fiber (utilizing center of mass locations) vs. the magnitude of the average velocity of each fiber. The data points appear to take on a Gaussian shape (see Fig. 2). We performed a Gaussian curve-fit through the data. The data points and best-fit Gaussian curve are plotted in Fig. 2. This simulation was performed several hundred times with different initial random networks, and random motion of a central fiber. The average Gaussian curve of best fit from these simulations is shown in Fig. 2, along with the Gaussians that utilize $\sigma \pm SD$ (standard deviation of σ). When utilizing a Gaussian curve for the frictional potential in our mesoscopic model, we will need to choose an appropriate value for σ . In the numerical experiments shown later in the paper, a value for σ was chosen based on simulations performed with the microscopic model (as above) where the parameters for the test case were utilized (see Table 1). In general we note that σ depends on several parameters such as the network's density, fiber length, and the upper limit of cross-link interaction distance R . A full parameter space investigation will be conducted in future work. Again for the numerical tests presented later, we ran the microscopic simulation multiple times (with different random networks) and computed the average σ value from these simulations, and utilized this value in the particle model simulations.

We now return to Eqs. (1a) and (1b) to look at the third term. The sum with $U'_e(r_{ij})$ represents the total elastic force acting on fiber i based on its direct cross-link interactions with other fibers. The idea is that a virtual spring appears between two fibers i and j whenever r_{ij} is below a given threshold distance R . If r_{ij} is greater than R then fibers i and j do not directly interact elastically, and no contribution is made to the sum. This "on-off" switch behavior is reflected in the structure of the $U'_e(r_{ij})$ potential function

$$U_e(r_{ij}) = \begin{cases} \frac{1}{2}k_0(r_{ij} - r_0)^2 - \frac{1}{2}k_0(R - r_0)^2 & r_{ij} < R, \\ 0 & r_{ij} \geq R, \end{cases} \quad (2)$$

where k_0 is the spring constant of a cross-link, and r_0 is the cross-link equilibrium length. This set-up of the elastic interaction model easily allows the model to capture cross-link rupture (if r_{ij} transitions from less than R to greater than R) and cross-link reformation (if r_{ij} transitions from greater than R to less than R). The cross-link interaction distance R depends in general on the geometrical properties of the network constituents such as typical fiber length, fiber orientation and the typical binding mechanism length (actin-binding protein typical length). For simplicity, in the numerical simulations R will be assumed constant and ranging between the typical length of binding proteins ≈ 50 nm and the typical length of actin fibers ≈ 2 μ m. The parameter λ_2 (like λ_1) is an adjustable parameter relating to the elastic behavior of the network. In Fig. 3 we show a plot of the elastic potential and elastic force generated between fiber i and j . This force function has repulsive, attractive and rupture zones in the cross-link behavior. In Eq. (1b), the final term $\mathbf{F}(t, \mathbf{x}_i)$ represents any external forces imposed on the fiber. Conceptually, Eqs. (1a) and (1b) represent a *Kelvin-Voigt* model between any pair of fibers having a viscosity of value $\frac{\lambda_1}{n} U_{fr}(r_{ij})$ and elasticity of $\frac{\lambda_2}{n} U'_e(r_{ij})$ as depicted in Fig. 1 (right).

The equations for the evolution of θ_i and ω_i have a similar structure to Eqs. (1a) and (1b). To derive the equation for ω_i , we use the angular conservation of momentum equation:

$$\frac{d\mathbf{L}_i}{dt} = \boldsymbol{\tau}_i.$$

where \mathbf{L}_i is the total angular momentum and $\boldsymbol{\tau}_i$ is the torque. \mathbf{L}_i can be computed as

$$\begin{aligned} \mathbf{L}_i &= \mathbf{x}_i \times (m\mathbf{v}_i) + \sum_{k=1,2} \mathbf{x}_i^k \times \frac{m}{2} \mathbf{v}_i^k \\ &:= \mathbf{x}_i \times (m\mathbf{v}_i) + I\boldsymbol{\omega}_i, \end{aligned} \quad (3)$$

where I is the moment of inertia for the fiber with respect to \mathbf{x}_i , its center. The vectors \mathbf{x}_i^k , \mathbf{v}_i^k for $k = 1, 2$ are the position and velocity of the fiber's two ends, and $\boldsymbol{\omega}_i$ is the angular velocity vector. On the one hand, differentiating equation (3) in time gives

$$\boldsymbol{\tau}_i = \frac{d\mathbf{L}_i}{dt} = \mathbf{x}_i \times \mathbf{F}^{\text{tot}} + I \frac{d\boldsymbol{\omega}_i}{dt}. \quad (4)$$

On the other hand, computing the torque directly

$$\begin{aligned} \boldsymbol{\tau}_i &= \left(\mathbf{x}_i + \frac{\ell_i}{2} \right) \times \mathbf{F}^1 + \left(\mathbf{x}_i - \frac{\ell_i}{2} \right) \times \mathbf{F}^2 \\ &= \mathbf{x}_i \times (\mathbf{F}^1 + \mathbf{F}^2) + \frac{\ell_i}{2} \times (\mathbf{F}^1 - \mathbf{F}^2) \\ &= \mathbf{x}_i \times \mathbf{F}^{\text{tot}} + \frac{\ell_i}{2} \times (\mathbf{F}^1 - \mathbf{F}^2), \end{aligned} \quad (5)$$

where \mathbf{F}^k , with $k \in \{1, 2\}$, are the total forces exerted on each end of the fiber and $\ell_i = \mathbf{x}_i^1 - \mathbf{x}_i^2$. Comparing equations (4) and (5) leads to

$$I \frac{d\boldsymbol{\omega}_i}{dt} = \frac{\ell_i}{2} \times (\mathbf{F}^1 - \mathbf{F}^2).$$

These forces include both internal and external forces. For the external force component introduce the force field $\mathbf{F}(t, \mathbf{x})$. Thus,

$$(\mathbf{F}^1 - \mathbf{F}^2)_{\text{ext}} = \mathbf{F}(t, \mathbf{x}_i^1) - \mathbf{F}(t, \mathbf{x}_i^2) =: \Delta\mathbf{F}(t, \mathbf{x}_i).$$

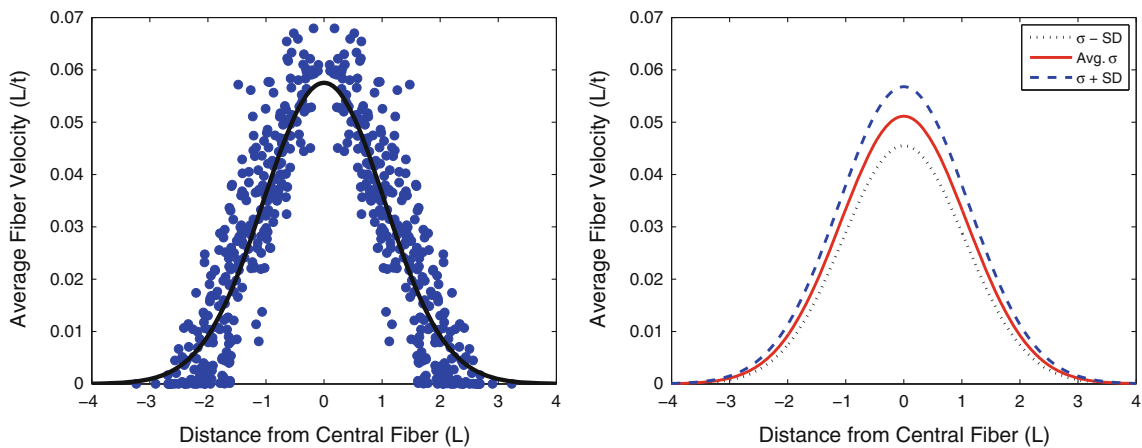


FIGURE 2. (Left) Blue points represent the average velocity of each fiber in a network vs. each fiber's distance to a central fiber. This central fiber has been randomly displaced to create a perturbation in the network that was originally in a state of mechanical equilibrium. The curve is the Gaussian best-fit curve through the data. (Right) The Gaussian curves that utilize the average value of σ and $\sigma \pm SD$ (standard deviation), where these statistics were computed from the results of several hundred runs of the experiment depicted in the left plot. The horizontal axis is normalized with respect to fiber length L .

TABLE 1. Parameter values utilized in the numerical simulations, determined from experimental papers.

Parameter	Symbol	Value in simulation
Filament length	L	$1 \mu\text{m}$
Filament width	a	8 nm
Cross-link equilibrium length	r_0	70 nm
Cross-link spring constant	k_0	10^{-6} N/m
Filament mass	m	$2.788 \times 10^{-17} \text{ g}$
Fluid viscosity	μ	$2 \times 10^{-2} \text{ Pa} \cdot \text{s}$

Parameters L , a , μ are utilized in computing $\beta_{1,2}$.

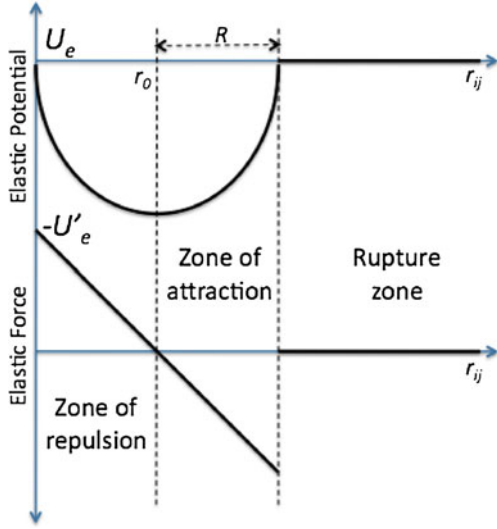


FIGURE 3. Elastic potential and force between fibers i and j .

Therefore,

$$\begin{aligned} \frac{\ell_i}{2} \times (\mathbf{F}^1 - \mathbf{F}^2)_{\text{ext}} &= \frac{L}{2} (\cos(\theta_i), \sin(\theta_i), 0) \times \Delta \mathbf{F}(t, \mathbf{x}_i) \\ &= \frac{L}{2} \Delta \mathbf{F}(t, \mathbf{x}_i) \cdot (-\sin(\theta_i), \cos(\theta_i), 0) \hat{\mathbf{e}}_3, \end{aligned}$$

where $\hat{\mathbf{e}}_3 = (0, 0, 1)$. For the internal force component, we use a friction term analogous to the one used in Eq. (1b) for the translational movement. That is, we prescribe that

$$\frac{\ell_i}{2} \times (\mathbf{F}^1 - \mathbf{F}^2)_{\text{int}} := -\frac{\lambda_3}{n} \sum_{j=1}^n U_{\text{fr}}(r_{ij})(\mathbf{w}_i - \mathbf{w}_j),$$

where $U_{\text{fr}}(r_{ij})$ is assumed to have the same Gaussian form as the translational case. Here we have neglected the rotational elastic component which could be added depending on the specific application. This term models the rotational friction forces between neighboring fibers or the fibers tendency to rotate together depending on the forces exerted on them. The parameter λ_3 is a rotational friction coefficient analo-

gous to the λ_2 parameter. Noticing that the angular velocity is defined as $\mathbf{w} =: \omega \hat{\mathbf{e}}_3$ one obtains a complete system of equations for the particle model of the fiber network:

$$\frac{d\mathbf{x}_i}{dt} = \mathbf{v}_i, \quad (6a)$$

$$\frac{d\theta_i}{dt} = \omega_i, \quad (6b)$$

$$\begin{aligned} m \frac{d\mathbf{v}_i}{dt} &= -\beta_1 \mathbf{v}_i - \frac{\lambda_1}{n} \sum_{j=1}^n U_{\text{fr}}(r_{ij})(\mathbf{v}_i - \mathbf{v}_j) \\ &\quad - \frac{\lambda_2}{n} \sum_{j=1}^n U'_e(r_{ij}) \frac{\mathbf{x}_i - \mathbf{x}_j}{r_{ij}} + \mathbf{F}(t, \mathbf{x}_i), \end{aligned} \quad (6c)$$

$$\begin{aligned} I \frac{d\omega_i}{dt} &= -\beta_2 \omega_i - \frac{\lambda_3}{n} \sum_{j=1}^n U_{\text{fr}}(r_{ij})(\omega_i - \omega_j) \\ &\quad + \frac{L}{2} \Delta \mathbf{F}(t, \mathbf{x}_i) \cdot (-\sin(\theta_i), \cos(\theta_i)), \end{aligned} \quad (6d)$$

where the terms $\beta_2 \omega_i$ represents rotational drag forces from the surrounding fluid on the fiber. Although only distance based potentials have been used to define system (6a, 6b), this is not a restriction of the model since more complicated ones are perfectly valid. For instance, angular dynamics of the fibers can strongly influence the translational dynamics by using anisotropic potentials $U(r_{ij}, \theta_{ij})$, in this way it is possible to consider anisotropic shear and stronger alignment effects. Furthermore, virtually any microscopic or macroscopic quantity such as fiber velocity, local density or temperature can be included as a valid variable in the potentials. This flexibility could potentially resolve local complex effects appearing in shearing like bending or bucking without including more degrees of freedom per fiber.

Qualitative Analysis of Equilibria

The evolution of the ordinary differential equation (ODE) System (6a, 6b) is highly dependent upon the shape of the potential functions $U_{\text{fr}}(r_{ij})$ and $U_e(r_{ij})$. In our case the friction potential $U_{\text{fr}}(r_{ij})$ is nonnegative and decays as the distance between fibers i and j increases. The elastic force is similar to that of Fig. 3 with one equilibrium state, meaning there exists a point $r_0 > 0$ such that $U'_e(r_0) = 0$ and

$$U_e(r_{ij}) = U_e(r_0) + \frac{k_0}{2} (r_{ij} - r_0)^2 + o(r_{ij} - r_0).$$

Here we give a qualitative analysis of the *free-driven* network's dynamical behavior (neglecting external

forces $\mathbf{F}(t, \mathbf{x}_i)$). We assume a well-formed network, that is, any two interacting fibers i, j satisfy $|\mathbf{x}_i - \mathbf{x}_j| \approx r_0$. We introduce the center of mass \mathbf{x}_c and momentum \mathbf{p}_c of the system:

$$\mathbf{x}_c = \sum_{i=1}^n \mathbf{x}_i, \text{ and } \mathbf{p}_c = m \sum_{i=1}^n \mathbf{v}_i.$$

We also introduce the kinetic and potential energies,

$$\begin{aligned} K &:= \frac{m}{2} \sum_{i=1}^n |\mathbf{v}_i|^2, \text{ and } P := \frac{1}{2n} \sum_{i,j=1}^n |\mathbf{x}_i - \mathbf{x}_j|^2 \\ &= \sum_{i=1}^n |\mathbf{x}_i|^2 - \frac{1}{n} |\mathbf{x}_c(0)|^2. \end{aligned}$$

Following the computations in Ha and Tadmor¹⁹ one finds, using the even symmetry of the potentials, that $\mathbf{p}_c(t) = \mathbf{p}_c(0) = 0$, $\mathbf{x}_c(t) = \mathbf{x}_c(0)$. Taking equation (6c) and multiplying it by \mathbf{v}_i and summing over i , we obtain:

$$\begin{aligned} \frac{dK}{dt} &= -\beta_1 \sum_{i=1}^n |\mathbf{v}_i|^2 - \frac{\lambda_1}{2n} \sum_{i,j=1}^n U_{\text{fr}}(|\mathbf{x}_i - \mathbf{x}_j|) |\mathbf{v}_i - \mathbf{v}_j|^2 \\ &\quad - \frac{\lambda_2}{2n} \sum_{i,j=1}^n \nabla U_e(|\mathbf{x}_i - \mathbf{x}_j|) \cdot (\mathbf{v}_i - \mathbf{v}_j). \end{aligned} \quad (7)$$

Understanding the symbol $1_{\{\cdot\}}$ as the indicator function of $\{\cdot\}$, we make the following approximations

$$U_{\text{fr}}(|\mathbf{x}_i - \mathbf{x}_j|) \approx U_{\text{fr}}(r_0) 1_{\{|\mathbf{x}_i - \mathbf{x}_j| \leq R\}} =: v_0 1_{\{|\mathbf{x}_i - \mathbf{x}_j| \leq R\}},$$

where v_0 is the equilibrium friction coefficient and R is an interaction distance. In addition,

$$\nabla U_e(|\mathbf{x}_i - \mathbf{x}_j|) \approx k_0 \left(1 - \frac{r_0}{|\mathbf{x}_i - \mathbf{x}_j|}\right) (\mathbf{x}_i - \mathbf{x}_j) 1_{\{|\mathbf{x}_i - \mathbf{x}_j| \leq R\}}.$$

Thus, the first and second terms in Eq. (7) become:

$$\begin{aligned} \beta_1 \sum_{i=1}^n |\mathbf{v}_i|^2 &= \frac{2\beta_1}{m} K \\ \frac{\lambda_1}{2n} \sum_{i,j=1}^n U_{\text{fr}}(|\mathbf{x}_i - \mathbf{x}_j|) |\mathbf{v}_i - \mathbf{v}_j|^2 &\approx 2\lambda_1 \frac{n_R v_0}{nm} K, \end{aligned}$$

where n_R is the number of interacting particles which we have assumed constant in time.

We have neglected the sum with cross terms in the friction term because

$$\begin{aligned} \sum_{i,j=1}^n \mathbf{v}_i \cdot \mathbf{v}_j 1_{\{|\mathbf{x}_i - \mathbf{x}_j| \leq R\}} &= \sum_{i,j=1}^n \mathbf{v}_i \cdot \mathbf{v}_j - \sum_{i,j=1}^n \mathbf{v}_i \cdot \mathbf{v}_j 1_{\{|\mathbf{x}_i - \mathbf{x}_j| > R\}} \\ &= - \sum_{i,j=1}^n \mathbf{v}_i \cdot \mathbf{v}_j 1_{\{|\mathbf{x}_i - \mathbf{x}_j| > R\}} \approx 0, \end{aligned}$$

In the last line we used the fact that $\mathbf{p}_c(t) = 0$ and $n \gg n_R$. Similar approximation is valid for $n_R \approx n$. For the third sum in Eq. (7)

$$\begin{aligned} &\frac{\lambda_2}{2n} \sum_{i,j=1}^n \nabla U_e(|\mathbf{x}_i - \mathbf{x}_j|) \cdot (\mathbf{v}_i - \mathbf{v}_j) \\ &\approx \frac{\lambda_2 k_0}{2n} \sum_{i=1}^n \sum_{|\mathbf{x}_i - \mathbf{x}_j| \leq R} \left(1 - \frac{r_0}{|\mathbf{x}_i - \mathbf{x}_j|}\right) (\mathbf{x}_i - \mathbf{x}_j) \cdot (\mathbf{v}_i - \mathbf{v}_j) \\ &= \frac{\lambda_2 k_0}{4n} \sum_{i=1}^n \sum_{|\mathbf{x}_i - \mathbf{x}_j| \leq R} \left(1 - \frac{r_0}{|\mathbf{x}_i - \mathbf{x}_j|}\right) \frac{d}{dt} |\mathbf{x}_i - \mathbf{x}_j|^2. \end{aligned}$$

This leads to the energy equation,

$$\begin{aligned} \frac{d}{dt} \left(K + \lambda_2 \frac{n_R k_0}{2n} P \right) &+ \left(\frac{2\beta_1}{m} + 2\lambda_1 \frac{n_R v_0}{nm} \right) K \\ &\approx \frac{\lambda_2 k_0 r_0}{2n} \frac{d}{dt} \sum_{i=1}^n \sum_{|\mathbf{x}_i - \mathbf{x}_j| \leq R} |\mathbf{x}_i - \mathbf{x}_j|. \end{aligned} \quad (8)$$

This energy relation implies that kinetic energy K dissipates with exponential rate $\frac{2\beta_1}{m} + 2\lambda_1 \frac{n_R v_0}{nm}$, where the first term is the dissipation rate of the surrounding fluid and the second is the intrinsic fiber network dissipation. Equation (8) also shows that the potential energy P is bounded. It is possible to say more by multiplying equation (6c) by \mathbf{x}_i and summing over i ,

$$\begin{aligned} m \frac{d}{dt} \sum_{i=1}^n \mathbf{x}_i \cdot \mathbf{v}_i &= 2K - \beta_1 \sum_{i=1}^n \mathbf{v}_i \cdot \mathbf{x}_i - \frac{\lambda_1}{2n} \\ &\quad \sum_{i,j=1}^n U_{\text{fr}}(|\mathbf{x}_i - \mathbf{x}_j|) (\mathbf{v}_i - \mathbf{v}_j) \cdot (\mathbf{x}_i - \mathbf{x}_j) - \frac{\lambda_2}{2n} \\ &\quad \sum_{i,j=1}^n \nabla U_e(|\mathbf{x}_i - \mathbf{x}_j|) \cdot (\mathbf{x}_i - \mathbf{x}_j) \approx 2K - \frac{\beta_1}{2} \frac{d}{dt} \\ &\quad \sum_{i=1}^n |\mathbf{x}_i|^2 - \frac{\lambda_1 v_0}{4n} \frac{d}{dt} \sum_{i=1}^n \sum_{|\mathbf{x}_i - \mathbf{x}_j| \leq R} |\mathbf{x}_i - \mathbf{x}_j|^2 - \frac{\lambda_2 k_0}{2n} \\ &\quad \sum_{i=1}^n \sum_{|\mathbf{x}_i - \mathbf{x}_j| \leq R} \left(1 - \frac{r_0}{|\mathbf{x}_i - \mathbf{x}_j|}\right) |\mathbf{x}_i - \mathbf{x}_j|^2. \end{aligned}$$

Expanding the sums one obtains the equation for the potential energy,

$$\begin{aligned} \frac{d^2 P}{dt^2} &+ \left(\frac{\beta_1}{m} + \lambda_1 \frac{n_R v_0}{nm} \right) \frac{dP}{dt} + 2\lambda_2 \frac{n_R k_0}{nm} P \\ &- \frac{4}{m} K \approx -2\lambda_2 \frac{n_R k_0}{n^2 m} |\mathbf{x}_c(0)|^2 + \frac{\lambda_2 k_0}{n m} \sum_{i=1}^n \sum_{|\mathbf{x}_i - \mathbf{x}_j| \leq R} \\ &\quad (2\mathbf{x}_i \cdot \mathbf{x}_j + r_0 |\mathbf{x}_i - \mathbf{x}_j|) \approx -2\lambda_2 \frac{n_R k_0}{n^2 m} |\mathbf{x}_c(0)|^2 \\ &\quad + \frac{\lambda_2 k_0 r_0^2 n_R}{m} + \frac{2\lambda_2 k_0}{n m} \sum_{i=1}^n \sum_{|\mathbf{x}_i - \mathbf{x}_j| \leq R} \mathbf{x}_i \cdot \mathbf{x}_j. \end{aligned} \quad (9)$$

Equation (9) shows that the dynamics of the network near equilibrium is described by a damped oscillator as intuition would suggest. The precise behavior can be designed with the choice of adjustment parameters $\lambda_{1,2}$ and the potentials, using Eq. (9). Observe the importance of the interaction range R for the dynamical behavior, furthermore, one can take $R \rightarrow \infty$, that is, $n_R \rightarrow n$ in Eq. (8) and (9) to obtain the behavior for long range interactions. In this case, Eq. (9) implies that the stationary potential energy is given by,

$$P_S := \lim_{t \rightarrow \infty} P(t) \approx \frac{nr_0^2}{2}.$$

As a simple test, we can compare simulation results from System (6a, 6b) (without external force terms), with the solution to the coupled ODE system in (8) and (9). Let us examine the simple case when $r_0 = 0$, $x_c(0) = 0$, and $n_R = n$. In this situation Eqs. (8) and (9) reduce to:

$$\frac{d}{dt} \left(K + \lambda_2 \frac{k_0}{2} P \right) + \left(\frac{2\beta_1}{m} + 2\lambda_1 \frac{v_0}{m} \right) K = 0 \quad (10a)$$

$$\frac{d^2 P}{dt^2} + \left(\frac{\beta_1}{m} + \lambda_1 \frac{v_0}{m} \right) \frac{dP}{dt} + 2\lambda_2 \frac{k_0}{m} P - \frac{4}{m} K = 0. \quad (10b)$$

Interpreting equations (10a) and (10b) as an approximation of a harmonic oscillator one may define the damping coefficient as

$$\zeta = \frac{\beta + v_0}{2\sqrt{2mk_0}},$$

where we just set $\lambda_1 = \lambda_2 = 1$. For the other variables we utilize typical parameters for an actin fiber network as a test case (See Table 1). We utilize 300 fibers in the simulation of System (6a, 6b). These 300 fibers are initially randomly assigned a position \mathbf{x}_i within a square domain centered around (0,0) of dimensions $R/2 \times R/2$ with $R = 1 \mu\text{m}$, so that all particles will interact with each other. All fibers have initial velocity $\mathbf{v}_i = 0$. With $r_0 = 0$ the equilibrium state for such a system is for all the particles to collapse down into a single point, therefore we should expect the potential energy of the system to eventually settle down to zero over time. Figure 4 shows graphs comparing the potential energy found in the solution of the ODE system in Eqs. (10a) and (10b) and the potential energy from the particle model in System (6a, 6b) calculated from particle positions. We ran the comparison for three cases: (1) where viscosity dominate over elasticity ($\zeta \gg 1$), (2) viscosity and elasticity have similar effect ($\zeta \approx 1$), and (3) elasticity dominates over viscosity ($\zeta \ll 1$). One can see that the results match very well in all 3 cases. An actin fiber network in a typical animal cell falls into the first category: an overdamped system,

typically dominated by cytosol fluid drag and internal friction.

BIOLOGICAL PARAMETERS FOR ACTIN NETWORKS

In the numerical tests presented below, we will utilize an actin fiber network as our test case. We now present the relevant biological parameters that will be utilized in these numerical experiments. Actin filaments are typically 0.2–20 μm long and 8 nm wide,^{6,10,25} with cross-links to other filaments appearing approximately every 100 nm along the filament's length.^{4,20,36} Individual actin filaments have a spring constant in the range of $4.5\text{--}6.5 \times 10^{-2}$ N/m,^{21,31} and typically only stretch 0.2–0.3% before rupturing.^{24,43} However the cross-linking proteins that create the network, tend to have lower spring constants, giving the overall network spring constants in the range of $10^{-6}\text{--}10^{-3}$ N/m depending on cross-link type.⁶ Also, the cross-linking proteins are normally in convoluted configurations when initially attached, so when force is applied to the network, these proteins can unfold, increasing their contour lengths and reducing tension.^{6,17}

Based on the molecular weight (42,000 Da) and size (125 nm^3) of an actin monomer, the mass density of the filament material is approximately 0.55 g/cm³.⁶ The density of filaments per unit volume, based on the number of filaments in a typical cell ($1\text{--}5 \times 10^5$)^{6,10} and the thickness of the actin network around the cell's periphery (0.2–2 μm),⁴¹ is estimated to be in the range 50 – 1000 filaments/ μm^3 . The fluid cytosol in which an actin network is suspended has a viscosity of $1 \times 10^{-3} \text{--} 2 \times 10^{-1} \text{ Pa} \cdot \text{s}$, with this wide range stemming from different measurement techniques and cell types.^{5,14,35} Table 1 shows a list of parameter values utilized in the simulations.

NUMERICAL TESTING

For the computational experiments presented below on strain hardening, network rupture, viscoelastic creep, stress relaxation, frequency response and network reformation, 300 fibers are instantiated in a domain region of dimension $L \times L$ where $L = 1 \mu\text{m}$. Each particle is assigned a random initial position vector \mathbf{x}_i within the confines of the domain. Each particle is also randomly assigned an orientation angle $\theta_i \in [-\pi/2, \pi/2)$. The velocity vector \mathbf{v}_i , as well as the angular velocity ω_i are initialized to zero. The ODE system in Eqs. (5)–(8) is evolved in time using a MATLAB solver. Prior to applying any external forces, the system is allowed to evolve to a state of mechanical equilibrium.

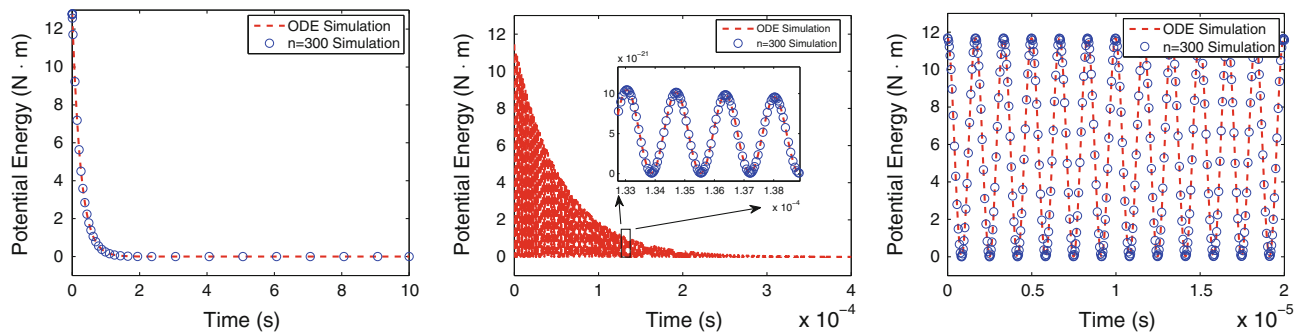


FIGURE 4. Comparison of the total potential energy computed for a simulation of System (6a, 6b) with 300 fibers, vs. the potential energy found as a solution to the ODE system in Eqs. (10a) and (10b) for the 3 cases of (from left to right) (1) viscosity dominates elasticity ($\zeta \gg 1$), (2) viscosity similar to elasticity ($\zeta \approx 1$), and (3) elasticity dominates viscosity ($\zeta \ll 1$). For an actin network, we have case (1), an overdamped system dominated by fluid drag and internal friction. (For visualization purposes, note the difference in time scales).

Strain Hardening

Strain hardening of actin networks has been demonstrated experimentally,^{15,45} and also by other computational models.^{4,16} There are several mechanisms for mechanical hardening, here we recreate two of them: (1) when the fiber block is strained say in the horizontal direction, the typical vertical distance between fibers tends to decrease. Consequently, cross-links are created mostly in the vertical direction which generates a configuration with more interconnected “parallel springs” than the initial configuration. In this way stiffness of the network increases in the strain direction, (2) consider again the situation in which the fiber block is strained in the horizontal direction, then the filaments tend to align themselves with the direction of strain in order to minimize their stored energy. This rearrangement creates a more parallel set of fibers and hence, the region of interaction between fibers increases. As a consequence, vertical cross-links are created generating again a configuration with more interconnected “parallel springs” than the original configuration.³⁹

Mechanism (1) is based on fiber’s vertical separation while mechanism (2) is based on the fiber’s orientation. Since a distance based elastic potential is used in the numerical experiments, only the effect of mechanism (1) is modeled. To demonstrate that our model exhibits such behavior, we begin with a block (size $L \times L$) of randomly placed and oriented fibers, that have been evolved to an equilibrium state. To insure that this first test does not include cross-link rupture, the threshold interaction distance is chosen of the same magnitude as the domain size $R = L$. The network is extensionally stretched in the horizontal direction, *via* the application of a constant, external force. During each step of the ODE evolution, the network’s strain and stored energy are computed. It has been shown in other models that at large strains, stretching is the dominant

contribution to network potential energy (as opposed to bending or torsion).³⁹ Thus the stored energy of the system at time step m is computed as:

$$E_m = \sum_{i=1}^n \sum_{j=1, j \neq i}^n \frac{1}{2} k_0 (r_{ij} - r_0)^2.$$

To estimate the overall spring constant κ_m of the block at time step m , an overall displacement D_m for the block is computed based on the average location of filaments near the left and right boundaries. We then estimate the network’s spring constant to be: $\kappa_m = 2 E_m / (D_m^2)$. A plot of the stored energy vs. strain is shown in Fig. 5, as well as a plot of the estimated spring constant κ_m of the network vs. strain. As expected the overall spring constant increases with the strain. Values for the overall network stiffness are in the 10^{-4} range, which falls in the range of measured values from Boal.⁶ As evidence that the model is also able to recreate mechanism (2) for strain hardening, Fig. 6 shows the initial distribution of filament angles, ranging from $[-\pi/2, \pi/2)$, and the angle distribution at 100% strain. The angles in this second histogram are grouped closer to zero, which is the angle at which the extensional force is being applied.

Network Rupture

To test the model’s ability to capture network rupture, which has been observed experimentally⁴⁶ and in other computational models,⁴ a similar experiment as the one described above is done, with the only modification that R is reduced to 140 nm. We begin again with a randomly positioned and oriented set of fibers in an $L \times L$ domain. The system is evolved to an equilibrium state and then the network is stretched with the same external force as above. The energy vs. strain plot and the network spring constant vs. strain

plot shown in Fig. 7 are quite different from Fig. 5. At first energy increases with strain, but then it begins to level off and decrease at larger strains, when cross-links between filaments begin to break. The overall spring constant of the network follows a similar pattern, increasing at first and then dropping as cross-links rupture at higher strains. Note that the energy stored in the network is considerably reduced with respect to that of previous experiment because of the choice of a smaller threshold interaction distance R , yet the estimated spring constant κ_m is remarkably similar before the network rupture as intuition suggests. Additionally, observe the network capability of enduring large strains without breaking apart, around 40% as shown in Fig. 7 (right). Such network's ability can be explained by the relatively large concentration of fibers which relocate to fill empty spaces making the average fiber separation relatively small in comparison to the overall strain. Figure 8 shows a series of snapshots of the network during this simulation.

Creep, Stress Relaxation and Frequency Response

We now perform some standard rheological tests to the square-shaped piece of material (of size $L \times L$) used in the previous sections. More specifically, we show creep, stress relaxation and frequency response of the model. A translational elastic quartic potential

$$U_e(r_{ij}) = \frac{k_0}{2}(r_{ij} - r_0)^2 + k_1(r_{ij} - r_0)^4 \quad (11)$$

is used for the numerical experiments instead of the quadratic potential (2) employed previously. Such approach was applied in Majumdar *et al.*³⁴ to enhance the nonlinear creep behavior in a semi-flexible chain and observe weak power law response $\sim t^\alpha$. The in-

crease of cell stiffness can be appreciated by computing the parameter α for systematically higher levels of mechanical stress and observing the decrease of such parameter. We recall here that α is an indicative of cell transition from elastic solid-like ($\alpha = 0$) to viscous fluid-like ($\alpha = 1$). In Fig. 9 (left) the creep response of a small piece of square-shaped viscoelastic material (size $L \times L$) is depicted for different tensile stresses applied in the horizontal direction using $k_1 = 10 k_0$.

Three regimes are differentiated: An initial fast response followed by a slower power law intermediate regime. Finally, the material reaches a steady state. In Fig. 9 (right) the transition to a solid-like material occurs as the mechanical stress is systematically increased. The parameter α can be easily manipulated by changing the size of the linear and nonlinear spring constants k_0, k_1 in the elastic potential.

In Fig. 10 (left) we show the stress relaxation response of the same square-shaped piece of material using again the quartic potential (11); in such experiment the strain is maintained constant until the network has reached a new stationary state as shown in Fig. 10. The relaxation is displayed using the normalized average stored potential energy of the material. The response is fitted with one of a standard linear solid (SLS) obtaining excellent agreement. This behavior does not contradict the nonlinear binding mechanism between fibers since we are displaying the collective (macro) response of these fibers. Similar exponential relaxation have been obtained in the literature (Fig. 4).³³

Figure 11 shows a low pass non-linear frequency response of the square-shaped viscoelastic material. This response is plotted over a large range of frequencies. In Fig. 11 (left) the ratio $\frac{\text{Strain}}{\text{Stress}}$ is plotted given a sinusoidal tensile stress input. In Fig. 11 (right) the

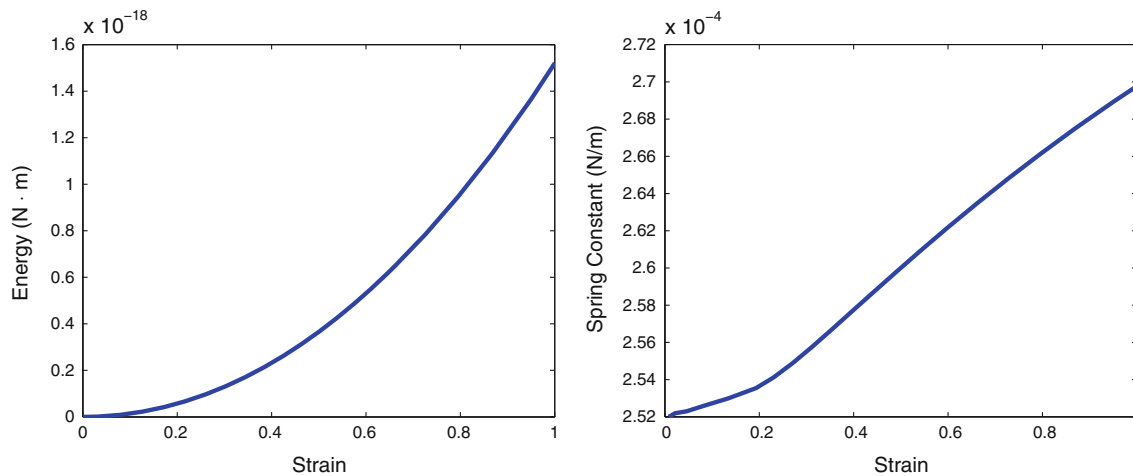


FIGURE 5. Energy vs. strain (left) and network spring constant vs. strain (right) as a demonstration of strain hardening of the network. In this simulation, cross-links are permanent (non-rupturing).

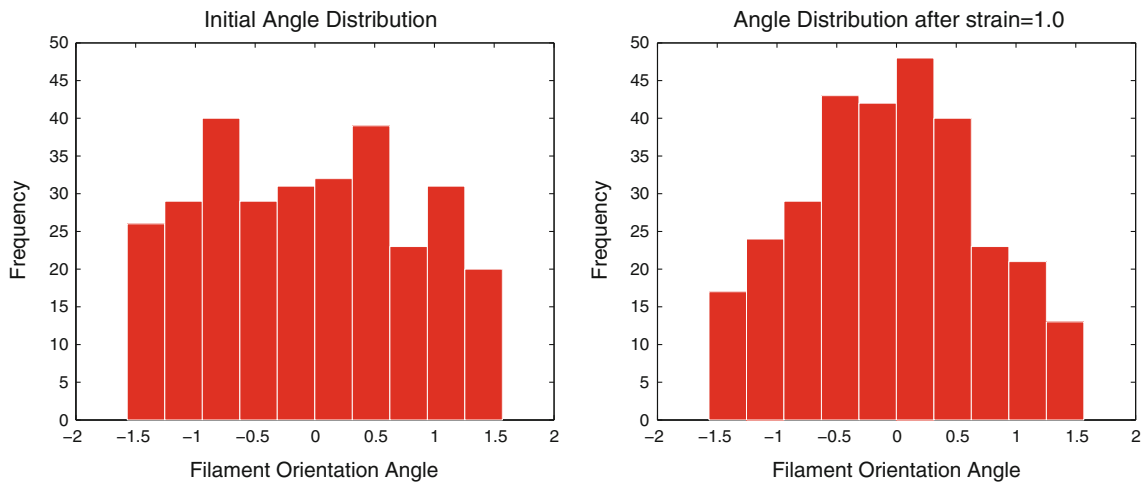


FIGURE 6. Distribution of filament angles (in radians) in the initial equilibrium state (left) and after 100% extensional strain (right).

phase delay between strain and stress is presented for the same experiment. The cut-off frequency of the magnitude response (≈ 0.2 Hz) is a measure of the transition from elastic to a viscous network.

Cytoskeletal Reformation

Since the potential functions are distance based, this model allows for the formation of new cross-links when two filaments get close enough to one another. To demonstrate this, we begin with two networks described with the elastic potential (2) and separated by a large enough distance ($> R = 140$ nm) to ensure there is no initial interaction between the two networks. These two networks are then moved towards each other by an external compressive force. Figure 12 shows snapshots of the two networks combining, forming new cross-links as they merge. Figure 13 shows the number of cross-links in the system over time as the two networks form one network.

Energy Transfer

The final scenario explored with this model was to investigate the mechanical transfer of energy through the network. Cellular activities such as blebbing, crawling and mechanotransduction rely on mechanical signals to initiate structural changes in the cytoskeletal network.^{14,38} Can mechanical changes such as contractions in the network propagate passively through the fiber network or must other active processes (e.g., chemical reactions, molecular motor processes) be involved in order to propagate energy?

To investigate this issue with our model, we begin with 400 fibers in a block of dimensions $L \times L$. To make this numerical experiment visually and quanti-

tatively clear, the 400 fibers are divided into 10 groups of 40 fibers. Each fiber in group $j = 1, \dots, 10$ is assigned the same x position, and a random y position, so that all fibers in group j fall into a column. These 10 columns are spaced 110 nm apart, and R is set to 100 nm. This means that the fibers only interact initially with the fibers in their column. To simulate the transfer of energy in this network, the first column of fibers at the far left of the block, is moved to the right by 100 nm, so that it is now only 10 nm to the left of the second column of fibers.

The fibers in these two columns are now close enough to interact and form cross-links. The distance between the two columns is shorter than the equilibrium length of a cross-link so the two columns will repel one another. This will start a chain reaction, where the second column will move towards the third, the third towards the fourth, etc. This simulation represents a compression wave in the network and is done for two cases: (1) viscosity dominate over elasticity $\zeta > 1$ (values in Table 1 used) and (2) elasticity dominates over viscosity $\zeta < 1$ (values in Table 1 used, except viscosity reduced). Figure 14 contains several snapshots of the fibers in the two cases as the wave passes through. What should be noted is that the wave fully passes through the elastic dominated system, but gets halted in the viscous dominated system. To determine if the wave in case (1) was simply slower (but still propagating) we simulated this case for a longer period of time, and found that column 4 is the furthest the wave goes. Table 2 gives the wave arrival time in column 4 and the maximum total kinetic energy of the particles in columns 2 and 4 between the two cases. The wave takes longer to arrive in column 4 for case (1) vs. case (2), which makes intuitive sense since the compressive wave is slowed down by drag and internal

Particle Interaction Model for the Simulation of Cross-Linked Networks

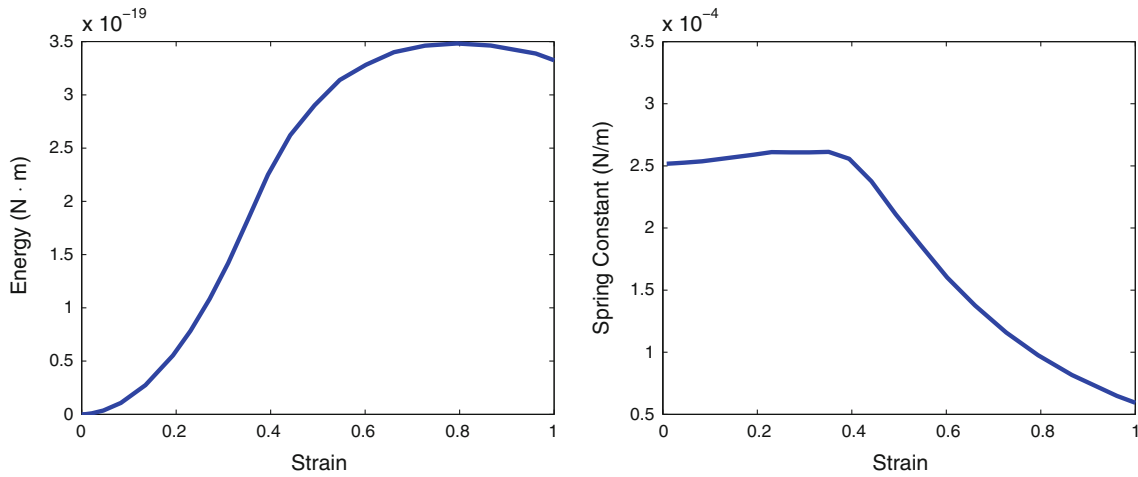


FIGURE 7. Energy vs. strain (left) and spring constant vs. strain (right) as a demonstration of network rupture in an actin fiber network. In this simulation, R is set to 140 nm.

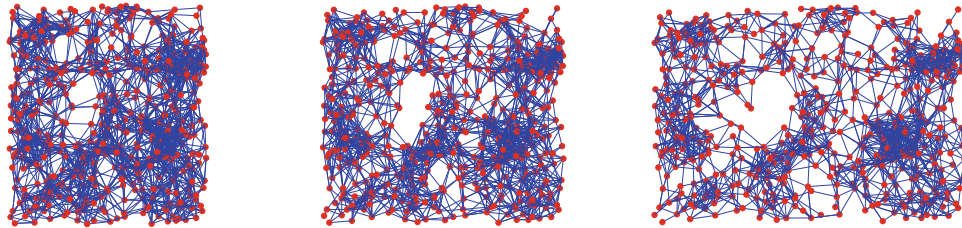


FIGURE 8. Snapshots of the network as its cross-links rupture when an extensional strain is applied to its left and right edges, at a slow strain rate. The red points are the center of mass positions of each fiber, and the blue lines represent cross-link connections between these fibers. As the network is extensionally strained, cross-links disappear as they are extended beyond the threshold interaction distance $R = 140$ nm.

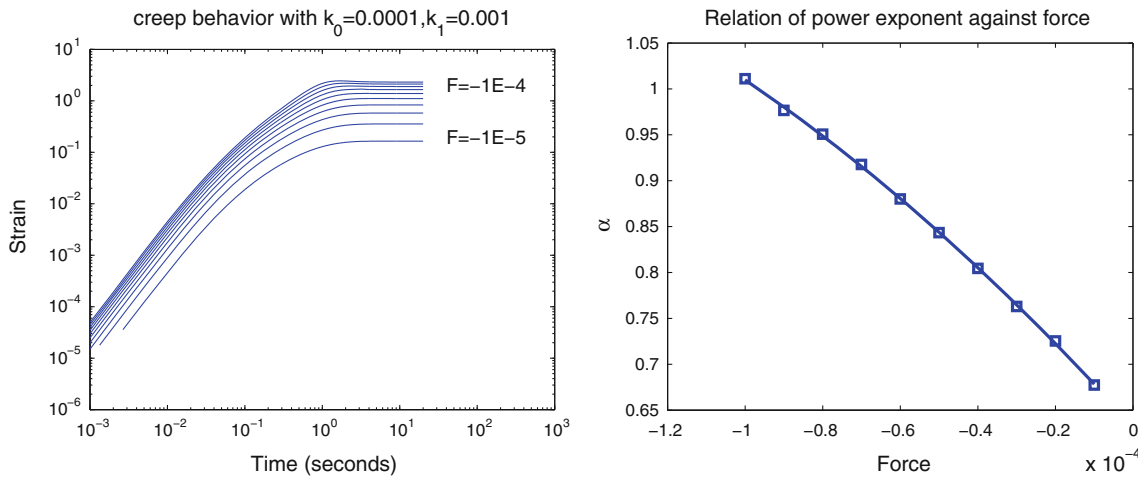


FIGURE 9. Creep response of small piece of viscoelastic material enduring different mechanical stresses (left). Cell stiffening, transition from viscous fluid-like to solid-like material as the stress increases (right).

friction. The kinetic energy in case (1) is much lower than in case (2), for columns 2 and 4, which again makes sense due to the greater energy dissipation in case (1).

Naturally, the speed of propagation and distance of energy propagation will depend on factors such as initial compressive strain placed on the block, density of fibers within the block, density of cross-links and

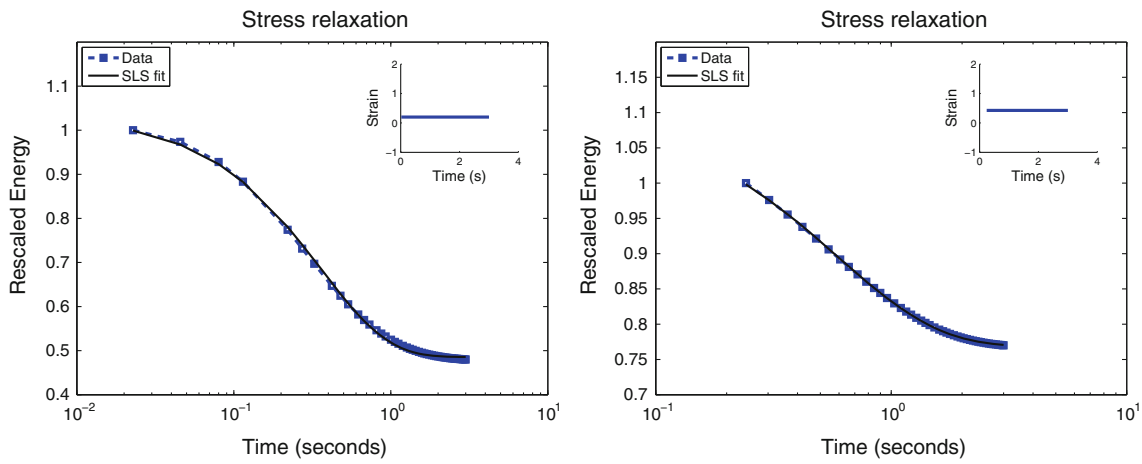


FIGURE 10. Stress relaxation for initial deformations of 20 and 50% with SLS fit (left and right respectively). A constant strain is applied until the network relaxes to a new state.

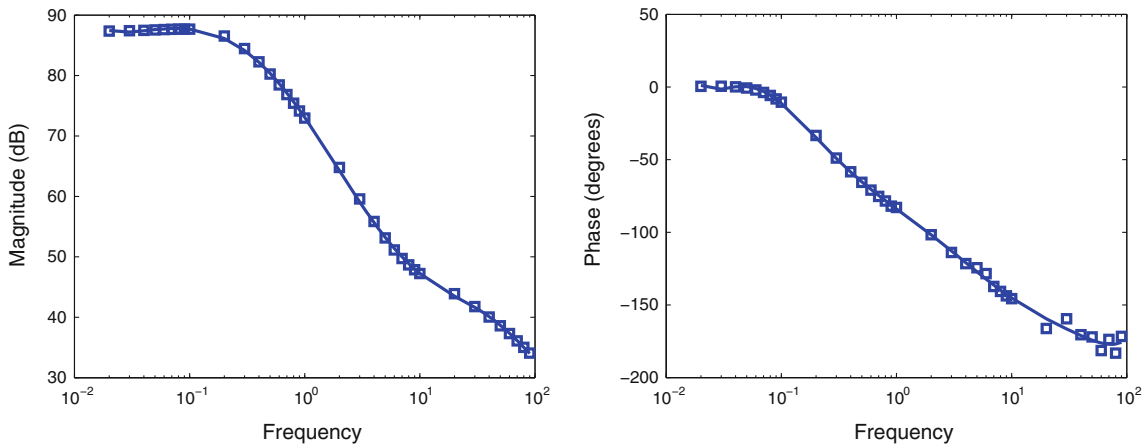


FIGURE 11. Frequency response of a square-shaped piece of viscoelastic material. Magnitude (left) and phase delay (right) response of the ratio $\frac{\text{Strain}}{\text{Stress}}$ for a sinusoidal tensile stress input.

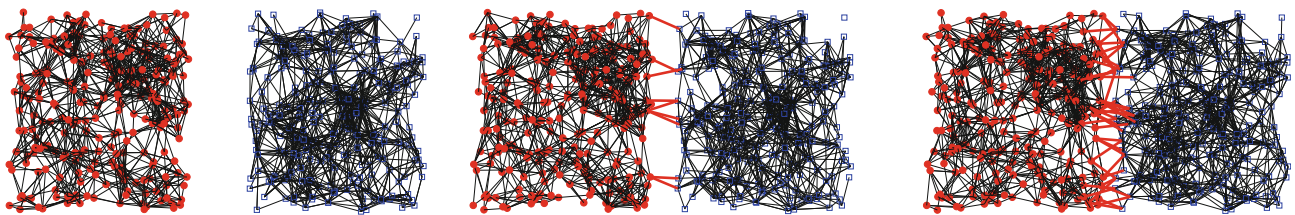


FIGURE 12. Snapshots of the network reformation, as two networks merge into one, as a compressive strain is applied at a slow strain rate to the left edge of the left network and the right edge of the right network. The red and blue points are the center of mass positions of each fiber for the left and right networks respectively. The black lines represent cross-link connections between fibers within the same network (left or right). The red lines represent cross-links that form between fibers from opposite networks. Cross-links form when two fibers become within $R = 140$ nm distance of each other.

the overall connectivity of the network. However, the main conclusion we draw from case (1), (where realistic actin network parameters have been used) is that viscosity and internal friction quickly damp energy waves, and this is not an efficient way for

energy to propagate across the cell. Energy can propagate locally within the network, but active processes such as biochemically induced acto-myosin contraction are needed for long-range energy transfer.

DISCUSSION AND PERSPECTIVE

A particle-interaction model for biological fiber networks has been developed. A “particle“ in this model is a fiber, and the fiber’s position, velocity, orientation angle, and angular velocity are the variables associated with each particle. In biological networks, fibers interact *via* cross-links and these connections can

often break and reform based on the cell or tissue’s need to reshape itself to perform various actions. These connections are represented in the model by distance-based potentials. The model is based on first principles for the conservative terms, and on a phenomenological model for the dissipative terms. The form of the friction potential term was chosen to be a Gaussian, and this choice was validated *via* a fully microscopic simulation of a fiber network.

To demonstrate the model’s ability to capture typical fiber network behaviors, an actin fiber network was chosen as a test case since there is a great deal of experimental data and results from other computational models available for this structure. The model was able to capture strain hardening, as filaments realign themselves to accommodate external stresses imposed on the network as well as meaningful viscoelastic response such as creep and stress relaxation. The model accounts for cross-link rupture and reformation, exhibiting similar behavior seen in polymer-based models.⁴ Finally we utilized the model to simulate the propagation of an energy wave across the network. For the actin network case, viscosity of the interstitial fluid and the network’s internal friction dominates, thus mechanical energy does not propagate very far from the source.

The major advantages of this mesoscale particle model over the fully microscopic polymer-based

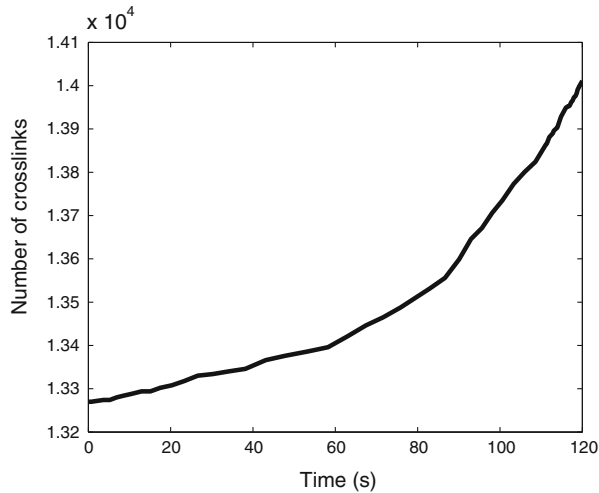


FIGURE 13. Number of currently existing cross-links within the network in Fig. 12 plotted over time as the two networks merge.

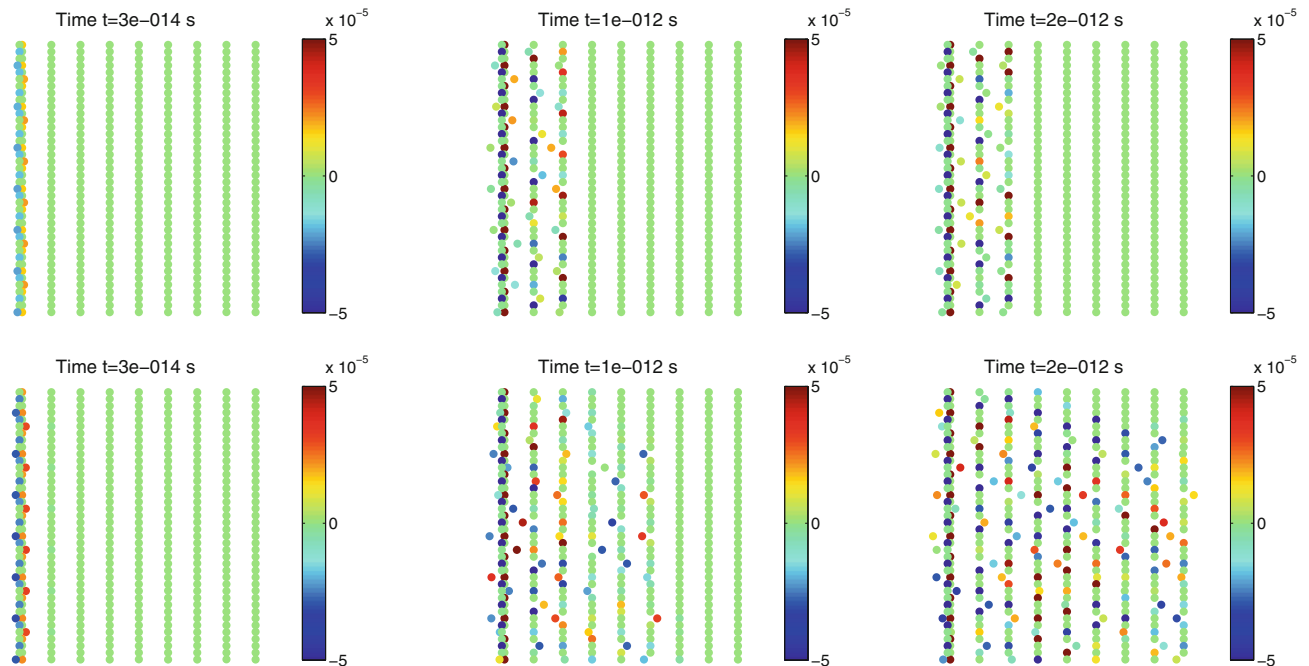


FIGURE 14. Snapshots in time of the fiber network as a compressive energy wave passes through for case (1) viscosity dominates over elasticity $\zeta > 1$ (top row) and case (2) elasticity dominates over viscosity $\zeta < 1$ (bottom row). The points represent center of mass positions for each fiber. The compressive force is applied to the first column of points only. The color of each particle represents the x velocity of that fiber in $\mu\text{m/s}$.

TABLE 2. Comparison of wave arrival times and kinetic energies in the two cases: (1) viscosity dominates over elasticity ($\zeta > 1$), (2) elasticity dominates over viscosity ($\zeta < 1$).

	$\zeta > 1$	$\zeta < 1$
Arrival time in 4	4.84e-13 s	2.02e-13 s
Kinetic energy in 2	9.41e-23 g · $\mu\text{m}^2/\text{s}^2$	8.8e-22 g · $\mu\text{m}^2/\text{s}^2$
Kinetic Energy in 4	1.36e-24 g · $\mu\text{m}^2/\text{s}^2$	9.29e-24 g · $\mu\text{m}^2/\text{s}^2$

models is three-fold. First of all, in our model one does not need to store in memory which fiber is attached to which other fibers, since this is taken care of by the potential functions which monitor current distances between all fibers. Secondly, all pertinent information about each fiber is incapsulated in six variable values (position, velocity, orientation) assigned to the particle that represents this fiber. In a polymer model, one would have many more degrees of freedom per fiber, slowing down the computation. Another advantage is that a particle model will be simple to couple with other physical phenomena, for example an exterior membrane or an interior fluid domain. These three advantages make the particle model computationally inexpensive to implement and run.

A final and important observation is that the particle model described by Eqs. (6a, 6b) possesses a *mean field limit*, that is, the model obtained for the distribution function of fibers $f(t, x, \theta, v, w)$ as the number of fibers is sent to infinity $n \rightarrow \infty$. It is well known that such model is given by the Boltzmann-like equation (see Bolley *et al.*⁸ and Ha and Tadmor¹⁹ for derivation),

$$\begin{aligned} \partial_t f + v \cdot \nabla_x f + w \partial_\theta f &= \beta_1 \nabla_v \cdot (vf) + \beta_2 \partial_w (wf) \\ &+ \nabla_v \cdot Q^T(f, f) + \partial_w Q^R(f, f), \end{aligned}$$

for appropriate translational and rotational interaction operators $Q^T(f, f)$ and $Q^R(f, f)$. This equation models an infinite network where each fiber pair interact with a chosen friction and elastic potentials such as the ones used in this manuscript. The mean field limit have several practical and theoretical advantages such as: (1) networks with large number of fibers can be resolved with little additional computational cost relative to the particle model, (2) maintains accuracy in dilute regimes as oppose to continuous models, (3) it can be naturally coupled with a background fluid equations through the viscosity coefficients β_1 and β_2 , therefore, accurate *macro-scale* simulations are achievable. Such scales are important to study for instance network buoyancy or cell scale phenomena such as blebbing, (4) thermal effects can be readily added with a Laplacian operator. Furthermore, active interactions can also be included by adding an interaction jump process operator of the type found in Aranson and Tsimring,³ and

(5) a continuous and simpler model enjoying (approximately) the properties presented in the numerical experiments can be derived from such mean field model in a classical and rigorous way.

REFERENCES

- ¹Alberts, B., A. Johnson, J. Lewis, M. Raff, K. Roberts, and P. Walter. *Molecular Biology of the Cell*, 4th ed. New York: Garland Science Press, 2002.
- ²Alt, W., and M. Dembo. Cytoplasm dynamics and cell motion: two-phase flow models. *Math. Biosci.* 156(1-2):207–28, 1999.
- ³Aranson, I. S., and L. S. Tsimring. Pattern formation of microtubules and motors: Inelastic interaction of polar rods. *Phys. Rev. E.* 71:050901(R), 2005.
- ⁴Aström, J. A., P. B. S. Kumar, I. Vattulaine, and M. Karttunen. Strain hardening in dense actin networks. *Phys. Rev. E.* 77(5):051913, 2008.
- ⁵Bicknese, S., N. Periasamy, S. Shohet, and A. Verkman. Cytoplasmic viscosity near the cell plasma membrane: measurement by evanescent field frequency-domain microfluorimetry. *Biophys. J.* 65(3):1272–1282, 1993.
- ⁶Boal, D. *Mechanics of the Cell*. New York: Cambridge University Press, 2002.
- ⁷Buxton, G. A., N. Clarke, and P. J. Hussey. Actin dynamics and the elasticity of cytoskeletal networks. *Express Polym. Lett.* 3(9):579–587, 2009.
- ⁸Bolley, F., J. A. Cañizo, and J. A. Carrillo. Stochastic mean-field limit: non-Lipschitz forces and swarming. *Math. Mod. Methods Appl. Sci.* 21:2179–2210, 2011.
- ⁹Callan-Jones, A. C., and F. Jülicher. Hydrodynamics of Active Permeating Gels. *New. J. Phys.* 13 093027, 2011.
- ¹⁰Cano, M. L., D. A. Lauffenburger, and S. H. Zigmond. Actin filament barbed-end capping activity in neutrophil lysates: the role of capping protein-beta 2. *J. Cell Biol.* 115(3):677–687, 1991.
- ¹¹Cucker, F., and S. Smale. Emergent behavior in flocks. *IEEE Trans. Automat. Control* 52:852–862, 2007.
- ¹²Chandran, P. L., and M. R. K. Mofrad. Rods-on-string idealization captures semiflexible filament dynamics. *Phys. Rev. E* 79:011906, 2009.
- ¹³Chandran, P. L., and M. R. K. Mofrad. Averaged implicit hydrodynamic model of semiflexible filaments. *Phys. Rev. E* 81:031920, 2010.
- ¹⁴Charras, G. T., M. Coughlin, T. J. Mitchison, and L. Mahadevan. Life and times of a cellular bleb. *Biophys. J.* 94(5):1836–1853, 2008.
- ¹⁵Chaudhuri, O., S. H. Parekh, and D. A. Fletcher. Reversible stress softening of actin networks. *Nature* 445:295–298, 2007.
- ¹⁶Chou, T. *Microstructural Design of Fibrous Composites*. New York: Cambridge University Press, 1992.
- ¹⁷Didonna, B. A., and A. J. Levine. Filamin cross-linked semiflexible networks: fragility under strain. *Phys. Rev. Lett.* 97(6):068104, 2006.
- ¹⁸Español, P., and P. Warren. Statistical mechanics of dissipative particle dynamics. *Europhys. Lett.* 30(4):191–196, 1995.
- ¹⁹Ha, S.-Y., and E. Tadmor. From particle to kinetic and hydrodynamic descriptions of flocking. *Kinet. Relat. Models* 1(3):415–435, 2008.

- ²⁰Head, D. A., A. J. Levine, and F. C. MacKintosh. Distinct regimes of elastic response and deformation modes of cross-linked cytoskeletal and semiflexible polymer networks. *Phys. Rev. E* 68(6):061907, 2003.
- ²¹Higuchi, H., T. Yanagida, and Y. E. Goldman. Compliance of thin filaments in skinned fibers of rabbit skeletal muscle. *Biophys. J.* 69(3):1000–1010, 1995.
- ²²Hoogerbrugge, P. J., and J. M. V. A. Koelman. Simulating microscopic hydrodynamic phenomena with dissipative particle dynamics. *Europhys. Lett.* 19(3):155–160, 1992.
- ²³Huisman, E. M., T. van Dillen, P. R. Onck, and E. Van der Giessen. Three-dimensional cross-linked F-actin networks: relation between network architecture and mechanical behavior. *Phys. Rev. Lett.* 99(20): 208103, 2007.
- ²⁴Huxley, H. E., A. Stewart, H. Sosa, and T. Irving. X-ray diffraction measurements of the extensibility of actin and myosin filaments in contracting muscle. *Biophys. J.* 67(6):2411–2421, 1994.
- ²⁵Janmey, P. A., J. Peetermans, K. S. Zaner, T. P. Stossel, and T. Tanaka. Structure and mobility of actin filaments as measured by quasielastic light scattering, viscometry, and electron microscopy. *J. Biol. Chem.* 261(18):8357–8362, 1986.
- ²⁶Joanny, J. F., F. Jlicher, K. Kruse, and J. Prost. Hydrodynamic theory for multi-component active polar gels. *New J. Phys.* 9(422):1–17, 2007.
- ²⁷Karcher, H., J. Lammerding, H. Huang, R. T. Lee, R. D. Kamm, and M. R. Kaazempur-Mofrad. A three-dimensional viscoelastic model for cell deformation with experimental verification. *Biophys. J.* 85(5):3336–3349, 2003.
- ²⁸Kim, T., W. Hwang, H., and R. D. Kamm. Computational analysis of a cross-linked actin-like network. *Exp. Mech.* 49:91–104, 2009.
- ²⁹Kim, T., W. Hwang, H. Lee, and R. D. Kamm. Computational analysis of viscoelastic properties of crosslinked actin networks. *PLoS Comput. Biol.* 5(7):e1000439, 2009.
- ³⁰Köhler, S., V. Schaller, and A. R. Bausch. Structure formation in active networks. *Nat. Mater.* 10:462–468, 2011.
- ³¹Kojima, H., A. Ishijima, and T. Yanagida. Direct measurement of stiffness of single actin filaments with and without tropomyosin by in vitro nanomanipulation. *Proc. Natl Acad. Sci. U.S.A.* 91:12962–12966, 1994.
- ³²Li, J., M. Dao, C. T. Lim, and S. Suresh. Spectrin-level modeling of the cytoskeleton and optical tweezers stretching of the erythrocyte. *Biophys. J.* 88(5):3707–3719, 2005.
- ³³Lieleg, O., J. Kayser, G. Brambilla, L. Cipelletti, and A.R. Bausch. Complex slow dynamics in bundled cytoskeletal networks. *Nat. Mater.* 10:236–242, 2011.
- ³⁴Majumdar, A., B. Suki, N. Rosenblatt, A. Alencar, and D. Stamenović. Power-law creep behavior of a semiflexible chain. *Phys. Rev. E.* 78(4):041922, 2008.
- ³⁵Mastro, A., M. Babich, W. Taylor, and A. Keith. Diffusion of a small molecule in the cytoplasm of mammalian cells. *Proc. Natl Acad. Sci. U.S.A.* 81(11):3414–3418, 1984.
- ³⁶Medalia, O., I. Weber, A. S. Frangakis, D. Nicastro, G. Gerisch, and W. Baumeister. Macromolecular architecture in eukaryotic cells visualized by cryoelectron tomography. *Science* 298(5596):1209–1213, 2002.
- ³⁷Mizuno, D., C. Tardin, C. F. Schmidt, and F. C. MacKintosh. Nonequilibrium mechanics of active cytoskeletal networks. *Science* 315(5810):370–373, 2007.
- ³⁸Mofrad, M. R. K. Rheology of the cytoskeleton. *Annu. Rev. Fluid Mech.* 41:433–453, 2009.
- ³⁹Onck, P. R., T. Koeman, T. van Dillen, and E. van der Giessen. Alternative explanation of stiffening in cross-linked semiflexible networks. *Phys. Rev. Lett.* 95(17):178102, 2005.
- ⁴⁰Pivkin, I., and G. Karniadakis. Accurate coarse-grained modeling of red blood cells. *Phys. Rev. Lett.* 101(11):118105, 2008.
- ⁴¹Sheetz, M. P., J. E. Sable, and H. Döbereiner. Continuous membrane-cytoskeleton adhesion requires continuous accommodation to lipid and cytoskeleton dynamics. *Annu. Rev. Biophys. Biomol. Struct.* 35:417–434, 2006.
- ⁴²Taber, L. A., Y. Shi, L. Yang, P. V. Bayly. A poroelastic model for cell crawling including mechanical coupling between cytoskeletal contraction and actin polymerization. *J. Mech. Mater. Struct.* 6:569–589, 2011.
- ⁴³Wakabayashi, K., Y. Sugimoto, H. Tanaka, Y. Ueno, Y. Takezawa, and Y. Amemiya. X-ray diffraction evidence for the extensibility of actin and myosin filaments during muscle contraction. *Biophys. J.* 67(6):2422–2435, 1994.
- ⁴⁴Walcott, S., and S. X. Sun. A mechanical model of actin stress fiber formation and substrate elasticity sensing in adherent cells. *PNAS* 107(17):7757–7762, 2010.
- ⁴⁵Xu, J., Y. Tseng, and D. Wirtz. Strain hardening of actin filament networks. Regulation by the dynamic cross-linking protein alpha-actinin. *J. Biol. Chem.* 275(46):35886–35892, 2000.
- ⁴⁶Yoon, Y., J. Kotar, G. Yoon, and P. Cicuta. Non-linear mechanical response of the Red Blood Cell. *Phys. Biol.* 5(3):36007, 2008.